Response to Reviewer RC2

Title: Two-dimensional Differential-form of Distributed Xinanjiang Model

Authors: Jianfei Zhao, Zhongmin Liang*, Vijay P. Singh, Taiyi Wen, Yiming Hu, Binquan Li, Jun Wang

Manuscript ID: hess-2024-377

We deeply appreciate your detailed review on our manuscript. All your comments have been carefully addressed, and a point-by-point response is provided below.

For better readability, the point-by-point response is formatted as follows:

- Reviewer's comments are shown in black
- Authors' responses are shown in blue
- Revisions to be incorporated in the revised manuscript are highlighted in red

Overall comments:

This manuscript not only summarizes the progress achieved during past decades but also advances the field by establishing a complete system of differential equations for the distributed XAJ model, along with its numerical implementation. The manuscript provides a thorough analysis of both one-dimensional and two-dimensional concentration methods while addressing numerical error issues. The manuscript is well-written with promising application prospects. To strengthen the manuscript, I would like to propose several comments in the order of line numbers.

Thank you very much for your concise paper summary and positive feedback on our research. We have carefully considered all of your comments and addressed them in the subsequent specific comments section. We hope that these changes could effectively address your concerns and enhance our manuscript.

Specific comments:

1. Line 55: It is more appropriate to describe this as "the widely-used three-water-sources lumped XAJ model."

Thanks for your suggestion. Including the term "three-water-sources" makes the sentence more precise. We will revise the sentence into:

"…, leading to the formation of the widely-used three-water-sources lumped XAJ model (Zhao, 1992)."

2. Line 56-66: While I agree the third phase highlighted the development of the distributed XAJ model,

it is important to note that the original lumped XAJ model has continued to evolve in parallel. The authors should briefly acknowledge this progression.

Thanks for pointing this out. We agree that it is important to acknowledge that the original lumped XAJ model has continued to evolve in parallel with the development of the distributed XAJ model. According to your suggestion, we will revise it to:

"**Phase 3 (2002-present):** The third phase is characterized by efforts to transition the XAJ model from a lumped to a distributed version, aligning it with other contemporary models like TOPMODEL and HBV (Beven et al., 2021; Seibert et al., 2022). It is noteworthy that the original lumped XAJ model has undergone continuous evolution alongside (Ouyang et al., 2025)."

3. Line 61: I believe the term "concentration method" is more appropriate here to maintain terminology consistency throughout the manuscript.

Thank you for your feedback regarding terminology consistency. We agree that aligning terminology strengthens clarity. In addition to Line 61, we have checked the terminology throughout the manuscript. The principle is to replace "route" with "runoff concentration" when used in conjunction with "runoff generation". According to your suggestion, we will revise it to:

"The transformation involved the application of the runoff generation modules to smaller computational units (e.g., sub-basins or grids) and implementing distributed hydrological or hydraulic runoff concentration methods (Chen et al., 2024; Fang et al., 2017; Liu et al., 2009; Su et al., 2003)."

4. Line 126: "Deeper" in Figure 1 should be corrected into "Deep", as referenced in Section 2.2.1. Besides, the slope-channel coupling diagram in this figure should be described in the text for clarity.

Thanks for pointing this out. As you suggested, we will revise it to:

"Line 122-127:
Water moves in two dimensions across the slope, with surface and subsurface runoff (interflow and groundwater) draining into the channels. The water in the channels is routed to the outlet in a one-dimensional flow pattern. Bidirectional water exchange between slope surface and channel is considered under varying hydraulic conditions. Specifically, when the channel water surface elevation is higher than that of the slope surface, water flows from the channel back onto the slope surface. The diagram of the TDD-XAJ is shown in Fig. 1.

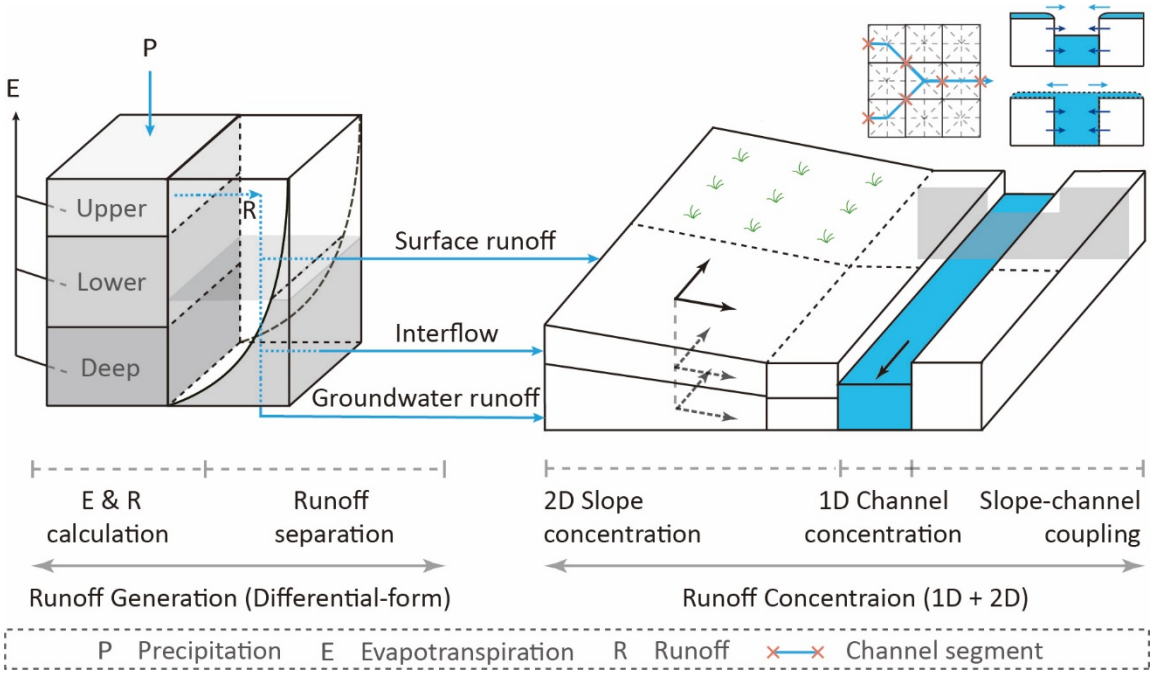

Figure 1. Diagram of the two-dimensional differential-form of distributed Xinanjiang model."

5. Line 145: The term "slope" is recommended instead of "hillslope".

Thanks for your suggestion. We will replace "hillslope" with "slope" accordingly and revise it into:

"Instead of the one-dimensional (1D) diffusion wave equations, the TDD-XAJ model employs two-dimensional (2D) diffusion wave equations to better represent surface water flow across the slope."

6. Line 153: Given the number of equations and variables, it is suggested to include a nomenclature section.

We agree that incorporating a nomenclature section would enhance readability, and we will include it in the form of supplementary material. Thanks for your suggestion.

7. Line 343: The determination methods of 15 model parameters listed in the Table 1 requires detailed explanation. In addition, it is also necessary to explain the differences in model parameter from the original XAJ model.

Thanks for your comments. The TDD-XAJ model comprises 15 parameters, which is one parameter more than the original lumped Xinanjiang model (Zhao et al., 2023), with 11 hydrological parameters for runoff generation and 4 parameters (2 hydrological and 2 hydraulic) for runoff concentration. These 13 hydrological parameters are consistent with those from the original lumped model. The remaining hydrological parameter of the original lumped model is used to represent the channel concentration

process. The channel concentration process is represented with one-dimensional diffusional wave equations in the TDD-XAJ model, thus transforming the hydrological parameter into a hydraulic parameter (channel roughness coefficient, n_c). The additional hydraulic parameter (surface roughness coefficient, n_s) in the TDD-XAJ model is included to facilitate two-dimensional diffusional wave equations for slope surface concentration.

We have added a column to the model parameter table (Table 5), to distinguish whether the parameters are spatially uniform or spatially distributed. For the spatially distributed parameters, we introduced their determination methods in the supplementary material (see Section S2). As suggested, we will revise it to:

"Line 343-344:
The TDD-XAJ model has 15 tunable parameters, which is one more than in the original lumped Xinanjiang model (Zhao et al., 2023). The signification and value range of these parameters are listed in Table 1. Parameters that can be spatially uniform are consistent with those from the original lumped model. The methods for determining spatially distributed parameters are provided in Sect. S2 of the Supplement.

Table 1. Parameters and parameter range of the TDD-XAJ model.

Components	Symbol	Signification	Range	Spatially	Unit
Evapotranspiration and runoff calculation	K_e	Coefficient of potential evapotranspiration to pan evaporation	[0.6, 1.5]	Uniform	-
	c	Coefficient of deep soil layer evapotranspiration	[0.01, 0.2]	Uniform/ Distributed	
	W_{um}	Tension water storage capacity of upper soil layer	[5, 30]	Uniform/ Distributed	mm
	W_{lm}	Tension water storage capacity of lower soil layer	[60, 90]	Uniform/ Distributed	mm
	W_{dm}	Tension water storage capacity of deep soil layer	[15, 60]	Uniform/ Distributed	mm
	A_{imp}	The ratio of the impervious area	[0.01, 0.2]	Uniform/ Distributed	-
	b	Tension water storage capacity curve exponent	[0.1, 0.4]	Uniform/ Distributed	-
Runoff separation	S_m	Free water storage capacity	[10, 50]	Uniform/ Distributed	mm
	ex	Free water storage capacity curve exponent	[1.0, 1.5]	Uniform/ Distributed	-
	K_i	Interflow outflow coefficient	[0.10, 0.55]	Uniform/ Distributed	-
	K_g	Groundwater outflow coefficient	$0.7 - K_i$	Uniform/ Distributed	-
Slope concentration	n_s	Surface roughness coefficient	[0.01, 0.80]	Distributed	m $s^{-1/3}$
	C_i	Interflow storage recession coefficient	[0.5, 0.9]	Uniform/ Distributed	-
	C_g	Groundwater storage recession coefficient	[0.98, 0.998]	Uniform/ Distributed	-
Channel concentration	n_c	Channel roughness coefficient	[0.01, 0.05]	Distributed	m $s^{-1/3}$

"

"**Section S2 of the Supplement:** The determination methods of spatially distributed model parameter

To determine spatially distributed model parameters, the process is generally based on spatially quantified data of watershed physical characteristics. This work is primarily carried out in two ways:
(1) **Lookup table-based method**. Parameters are determined from tables based on watershed physical

attributes. Specifically, the ratio of the impervious area (A_{imp}) and coefficient of deep soil layer evapotranspiration (c) are determined according to land use types (Yao et al., 2012), while the determination of tension water storage capacity curve exponent (b) and free water storage capacity curve exponent (ex) are assigned based on soil types. The value of surface roughness coefficient (n_{s}) is assigned based on the land use type of each grid cell, with different land uses corresponding to different roughness coefficients, which are derived from existing literature (Miao et al., 2016; Perrini et al., 2024). For channel roughness coefficient (n_{c}), values are obtained from a roughness coefficient table for river channels (Arcement and Schneider, 1989).

(2) **Physical meaning-based method**. Parameter values are calculated using quantitative watershed physical characteristics according to the physical meaning of the parameters. Specifically:

a. Tension water storage capacity of the upper, lower, and deep soil layer (W_{um}, W_{lm}, and W_{dm}). The summation of W_{um}, W_{lm}, and W_{dm} represents the tension water capacity of the entire soil layer (W_{m}), and it can be determined according to soil hydrological parameters and soil layer depth (Yao et al., 2012), which could be expressed as:

$$W_{\mathrm{m}} = (\theta_{\mathrm{f}} - \theta_{\mathrm{r}})D_{\mathrm{s}}, \tag{S4}$$

where θ_{f} is field capacity, θ_{r} is residual water content, D_{s} is soil layer depth (mm). Subsequently, two watershed-scale uniform coefficients (K_{um} and K_{lm}) and their derived value ($1 - K_{\mathrm{um}} - K_{\mathrm{lm}}$) are used to divide W_{m} into W_{um}, W_{lm}, and W_{dm} accordingly, which are given as:

$$W_{\mathrm{um}} = W_{\mathrm{m}}K_{\mathrm{um}}, \tag{S5}$$

$$W_{\mathrm{lm}} = W_{\mathrm{m}}K_{\mathrm{lm}}, \tag{S6}$$

$$W_{\mathrm{dm}} = W_{\mathrm{m}}(1 - K_{\mathrm{um}} - K_{\mathrm{lm}}). \tag{S7}$$

b. Free water storage capacity (S_{m}). S_{m} usually represents the capacity of free water in the humus layer. Thus, it can be determined according to soil hydrological parameters and the humus layer depth (Yao et al., 2012), which could be expressed as:

$$S_{\mathrm{m}} = (\theta_{\mathrm{s}} - \theta_{\mathrm{f}})D_{\mathrm{h}}, \tag{S8}$$

where θ_{s} is saturated water content, θ_{f} is field capacity, D_{h} is humus layer depth (mm).

c. Interflow and groundwater outflow coefficient (K_{i} and K_{g}). K_{i} and K_{g} represent the outflow rate of interflow and groundwater. The method for determining K_{i} and K_{g} involves converting the free water storage to corresponding saturated water depth, based on the hillslope storage-discharge theory and steady-state assumptions, which is then multiplied by the slope gradient and saturated hydraulic conductivity using the kinematic wave assumption (Tong, 2022). K_{i} and K_{g} are finally expressed as the ratios of corresponding flow distance in the time interval of input forces to the slope length, which could be given as:

$$K_{\mathrm{i}} = \frac{2S_0K_{\mathrm{su}}S_{\mathrm{hill}}\Delta T}{1000(\theta_{\mathrm{s}}-\theta_{\mathrm{f}})L_{\mathrm{hill}}^2}, \tag{S9}$$

$$K_g = \frac{2S_0 K_{sl} S_{hill} \Delta T}{1000(\theta_s - \theta_f) L_{hill}^2}, \quad \text{(S10)}$$

where S_0 is free water storage (mm), K_{su} and K_{sl} is saturated hydraulic conductivity of the upper (representing interflow) and lower (representing groundwater) soil layer respectively (m s^{-1}), S_{hill} is the gradient of the slope, ΔT is the time interval of input forces (s), and L_{hill} is the length of the slope (m).

d. Interflow and groundwater storage recession coefficient (C_i and C_g). C_i and C_g represent the time delay for interflow and groundwater runoff as they travel from specific locations on the slope to the river channel. These parameters are determined based on the theory of spatially distributed unit hydrograph (Maidment et al., 1996; Tong, 2022). The grid cells that form the flow path extending from specific locations on the slope to the river channel is first identified using GIS. Then, using the kinematic wave assumption, the flow velocity of interflow and groundwater runoff through each grid cell is computed based on the saturated hydraulic conductivity of the upper and lower layers and the slope gradient. Finally, the time taken for flow through each grid cell is accumulated, which could be expressed as:

$$T_i = \sum_{j=1}^{N_{hill}} L_{hill}^j / \left(K_{su}^j S_{hill}^j\right), \quad \text{(S11)}$$

$$T_g = \sum_{j=1}^{N_{hill}} L_{hill}^j / \left(K_{sl}^j S_{hill}^j\right), \quad \text{(S12)}$$

where T_i and T_g is the accumulated travel time from specific locations on the slope to the river channel through interflow and groundwater respectively (s), N_{hill} is the count of grid cells that form the flow path. C_i and C_g for each grid cell are further derived using theoretical conversion, which could be given as:

$$C_i = \exp(-\Delta T / T_i), \quad \text{(S13)}$$

$$C_g = \exp\left(-\Delta T / T_g\right). \quad \text{(S14)}$$

The primary data used to determine spatially distributed model parameters include soil physical and hydraulic properties, slope gradient, and land use. These can be obtained from open-source datasets, such as Harmonized World Soil Database v2.0 (HWSD v2.0) (FAO and IIASA, 2023), China dataset of soil properties for land surface modelling version 2 (CSDLv2) (Shi et al., 2025), and Global land cover mapping at 30m resolution (GlobeLand30) (Chen et al., 2015)."

8. Line 439: The equation of FVRE should be provided. Similarly, it is also suggested to provide the formulas of three channel cross-sectional hydraulic elements mentioned in Line 282.

Thanks for your comment. As you suggested, the equation of FVRE is provided below:

"The equation of FVRE could be given as:

$$\mathrm{FVRE} = \left(\sum_{i=1}^{n} Q_{sim,i} - \sum_{i=1}^{n} Q_{obs,i}\right) / \sum_{i=1}^{n} Q_{obs,i} * 100\% \quad (32)$$

where $Q_{sim,i}$ and $Q_{obs,i}$ represent simulated and observed discharge at time step i (m^3 s^{-1}), and n is the length of the sequence."

Furthermore, we will provide the formulas of three channel cross-sectional hydraulic elements (cross-sectional area, water surface width, and wetted perimeter) in supplementary material (see Section S1).

"**Section S1 of the Supplement:** Cross-sectional generalization and hydraulic parameters of river channel

In the two-dimensional differential-form of distributed Xinanjiang model (TDD-XAJ), the cross-section of river channel is generalized into a trapezoid (Fig. S1). Thus, the formulas for cross-sectional area, water surface width, and channel wetted perimeter could be given as:

$$A = \begin{cases} \varsigma h_c + {h_c}^2/\tan\beta & 0<\beta<90° \\ \varsigma h_c & \beta = 90° \end{cases}, \quad (S1)$$

$$B = \begin{cases} \varsigma + 2h_c/\tan\beta & 0<\beta<90° \\ \varsigma & \beta = 90° \end{cases}, \quad (S2)$$

$$\chi = \begin{cases} \varsigma + 2h_c/\sin\beta & 0<\beta<90° \\ \varsigma + 2h_c & \beta = 90° \end{cases}, \quad (S3)$$

where A is cross-sectional area (m^2), B is water surface width (m), χ is channel wetted perimeter (m), ς is channel bottom width (m), h_c is channel water depth (m), β is river bank slope gradient (°).

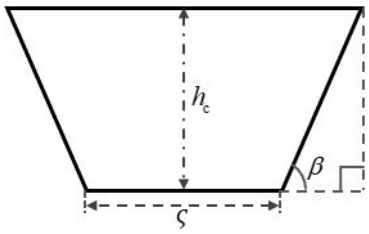

Figure S1. Diagram of trapezoidal cross-sectional generalization of river channel."

9. Line 452: In the slope concentration methods comparison experiment, the authors systematically compared the 1D and 2D forms of the diffusion wave and linear reservoir methods based on idealized test cases. For the diffusion wave method, significant differences were observed between the 1D and 2D form, both in terms of hydrographs and surface storage. However, for the linear reservoir method, while the differences in hydrographs were noticeable (Figure 6g and 6h), the contrast in storage was less evident (Figure 7b and 7d). The authors should improve the visualization approach for Figure 7 such as by changing color schemes to make the comparison more clear.

We are sorry for not clearly presenting the differences between the spatial distributions of interflow

storage simulated by the 1D and 2D linear reservoir methods, as also noted by other reviewers. Following the suggestion of reviewer CC1, we provide the complete spatial distribution of interflow storage and then zoom in on areas with significant differences. This approach allows for a clearer illustration while preserving data integrity. The revised Figure 7 is shown below:

"Line 452-457:

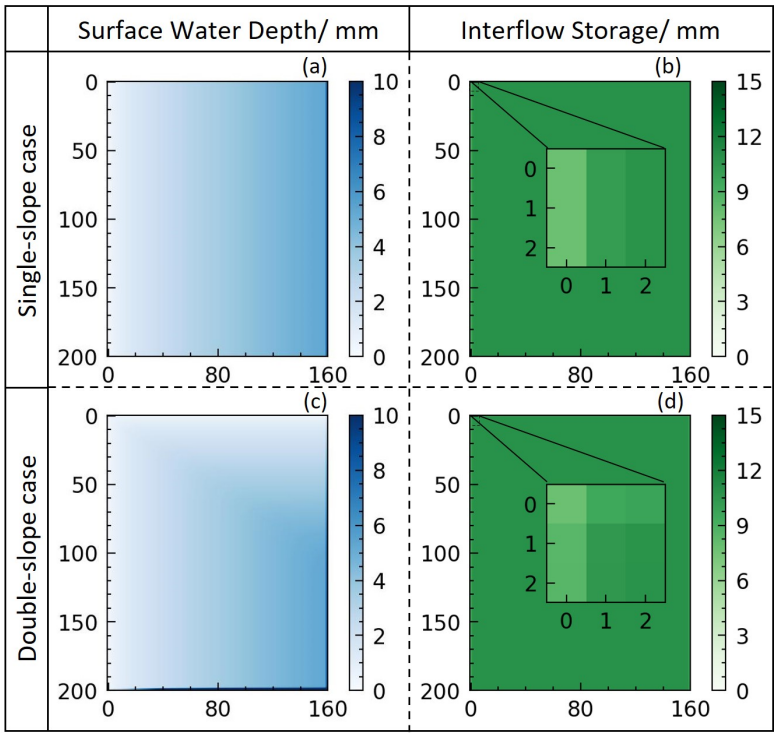

Figure 7. The spatial distribution of surface water depth (h_s) and interflow storage (O_i) on the left-side hillslope of both single-slope (a-b) and double-slope (c-d) synthetic V-catchment test cases at the 60 minute mark. The state variable distributions shown are simulated using two-dimensional (2D) slope concentration methods. The corresponding results of 1D methods are identical to those obtained from the single-slope case simulated with 2D methods, regardless of the test case used. For a clear comparison, the spatial distribution of O_i in the upper left corner has been zoomed."

10. Line 547-565: The authors analyzed the model's performance by applying it to the Tunxi watershed and examining the flow hydrograph at the outlet station, and the overall simulation results were satisfactory. However, as a distributed hydrological model, the authors should provide more details regarding the spatial simulation. Furthermore, it is suggested that the authors could include comparative results from stations within the watershed, if possible, as this would provide a more comprehensive evaluation of the performance of the TDD-XAJ model.

Thanks for your feedback on enhancing the spatial evaluation of the TDD-XAJ model. To address this, we have further included the spatial simulation results in addition to the simulated hydrograph in 2008 (Figure 10). Moreover, to strengthen the assessment of model performance, we introduced the Yuetan hydrological station—a station within the Tunxi watershed (Figure 5), and compared its simulation results

with observed data. Details of performance metrics are provided in Table 4. As shown in Table 4, the average values of the Nash-Sutcliffe efficiency (NSE), Kling-Gupta efficiency (KGE), the absolute flood volume relative error (|FVRE|), and the coefficient of determination (R^2) for Yuetan station (across all years) are 0.83, 0.78, 6.2%, and 0.86, respectively. The corresponding values for Tunxi station are 0.87, 0.80, 6.7%, and 0.90. In summary, these metrics indicate that the TDD-XAJ model provides robust streamflow simulations at both stations in the Tunxi watershed. The revisions to be implemented are shown below:

"Line 421:

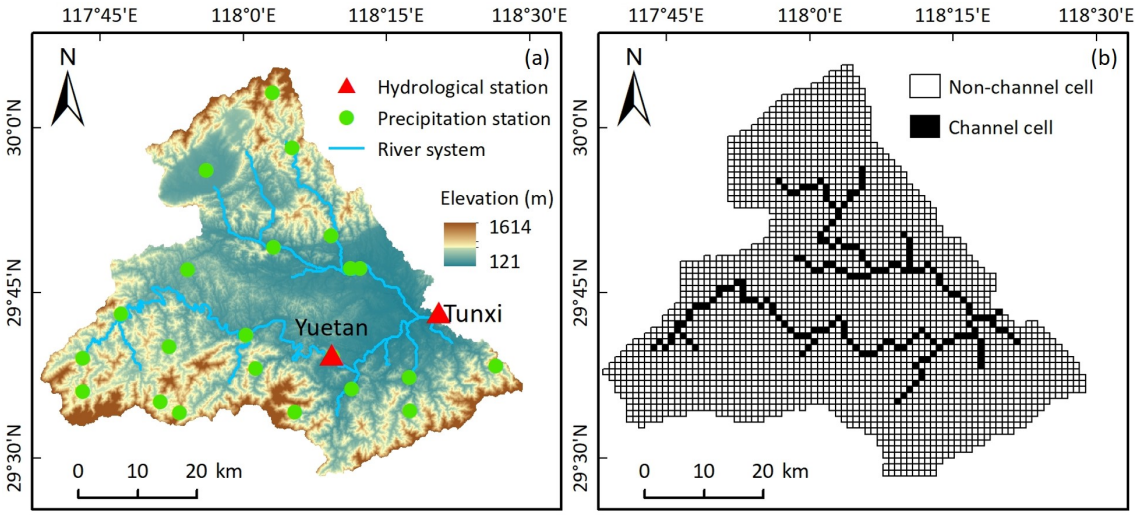

Figure 5. Location and gauging station distribution of the Tunxi watershed (a), and the spatial discretization of the watershed, including channel and non-channel cells (b)."

"Line 553-566:

Table 4. Annually evaluated simulation performance metrics of the TDD-XAJ model in the Tunxi watershed.

Period	Year	Tunxi				Yuetan			
		NSE	KGE	FVRE(%)	R^2	NSE	KGE	FVRE(%)	R^2
Calibration	2008	0.94	0.91	-8.26	0.94	0.90	0.89	-1.33	0.90
	2009	0.88	0.90	-6.95	0.88	0.82	0.80	-16.43	0.83
	2010	0.85	0.78	-16.88	0.90	0.82	0.78	-18.99	0.87
	2011	0.89	0.78	7.53	0.89	0.78	0.76	-3.46	0.80
	2012	0.82	0.84	-7.64	0.83	0.74	0.80	-5.97	0.74
	2013	0.87	0.80	-10.75	0.92	0.88	0.79	-3.99	0.92
	2014	0.88	0.79	0.20	0.91	0.84	0.75	0.72	0.87
Validation	2015	0.85	0.77	-9.92	0.92	0.85	0.80	-8.48	0.88
	2016	0.88	0.78	-6.92	0.92	0.86	0.79	-4.37	0.89
	2017	0.88	0.76	1.62	0.92	0.84	0.72	4.66	0.86
	2018	0.87	0.77	1.58	0.89	0.87	0.78	-2.75	0.90
	2019	0.85	0.74	-2.24	0.89	0.79	0.74	-3.70	0.81

For the outlet station of Tunxi watershed, Table 4 indicates that the values of the FVRE metric are all

within ±20 %. The absolute values of the FVRE (|FVRE|) averaging 8.3 % for the calibration period and 4.5 % for the validation period. In terms of hydrograph evaluation, the average values of NSE and KGE are 0.88 and 0.83 for the calibration period and 0.87 and 0.76 for the validation period, which is slightly better for the calibration period than for the validation period. The minimum value of R^2 is 0.83 for all years, and the average value for all years is 0.90. In a direct comparison, Tong (2022) conducted a similar daily simulation in the same watershed using the GXAJ model, reporting average NSE and |FVRE| values of 0.85 and 11.0% between 2008 and 2017, respectively. In contrast, the TDD-XAJ model achieved average values of 0.87 for NSE and 7.7% for |FVRE| in the same period. For the Yuetan station within Tunxi watershed, Table 4 shows that FVRE metric values remain within ±20 %. The average (|FVRE|) is 7.3 % and 4.8 % for the calibration and validation periods, respectively. Meanwhile, the average value of NSE is 0.82 for the calibration period and 0.84 for the validation period, and the average KGE is 0.80 and 0.77 for calibration period and validation period, respectively. Across all years, the average R^2 reaches 0.86.

Fig. 9 provides an example of the simulated hydrograph at Tunxi and Yuetan station of the TDD-XAJ model in 2008. We further analyzed the spatial simulation capability of the TDD-XAJ model using precipitation events from June 6-8, 2008, which occurred just before the flood peak and exhibited distinct spatial patterns (Fig. 10a-c). On June 6, almost no rainfall was recorded; on June 7, precipitation was concentrated in the upper-left corner; and on June 8, it was focused in the lower-right corner. The simulation results for tension and free water storage reflect these patterns. Specifically, on June 7 (Fig. 10d and 10g), the overall tension water storage was unsaturated with minimal free water storage. Subsequently, saturation of tension water occurred in the upper-left part of the watershed, and free water storage increased significantly in areas with heavier rainfall (Fig. 10e and 10h). On June 8, the tension water in the lower-right corner became fully saturated due to the coverage of precipitation (Fig. 10f). For free water (Fig. 10i), the storage in the same area also approached saturation, whereas the saturated areas in the upper part quickly dissipated due to the faster recession of free water.

The results indicate a good and consistent agreement between the observation and the simulations of the TDD-XAJ model in the Tunxi watershed, demonstrating a slight improvement in performance metrics compared to the GXAJ model, particularly for flood volume. Additionally, the spatial analysis of simulation results demonstrates that the TDD-XAJ model captures spatial variability in water storage effectively in response to varying precipitation patterns.

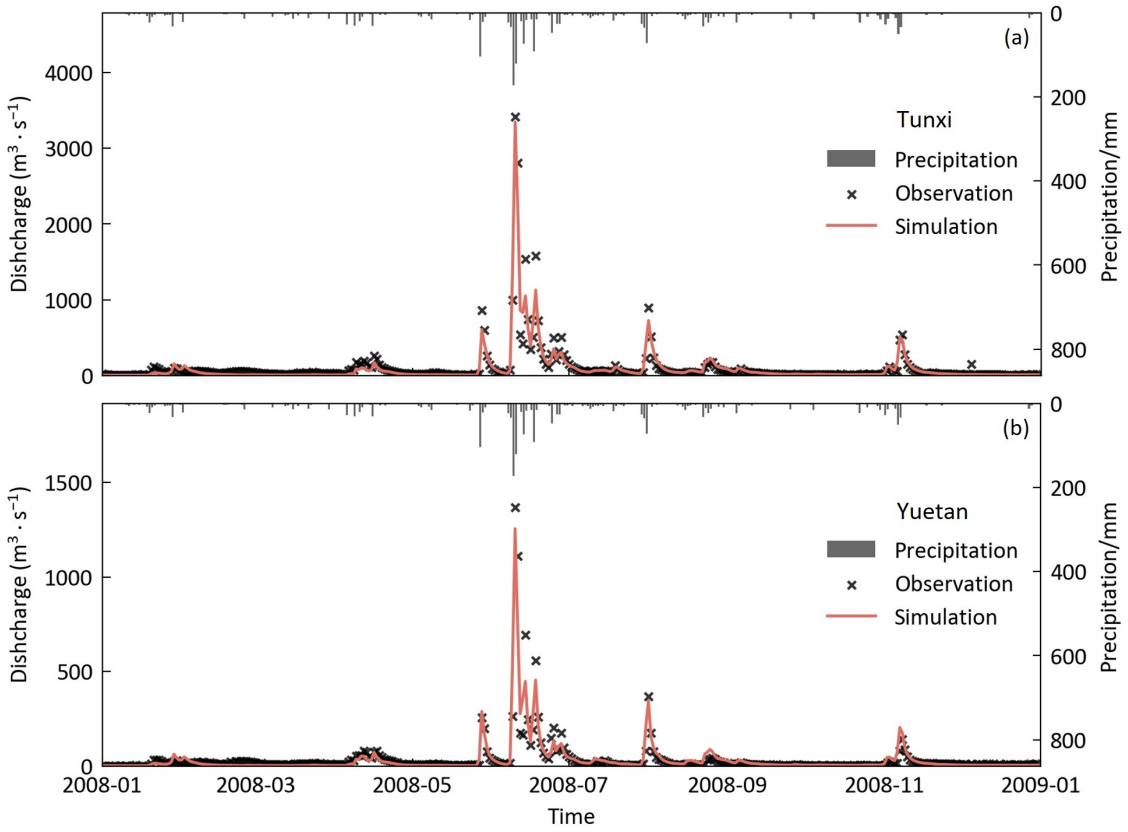

Figure 9. The simulated hydrograph at Tunxi (a) and Yuetan (b) station of the Tunxi watershed in 2008 using the TDD-XAJ model.

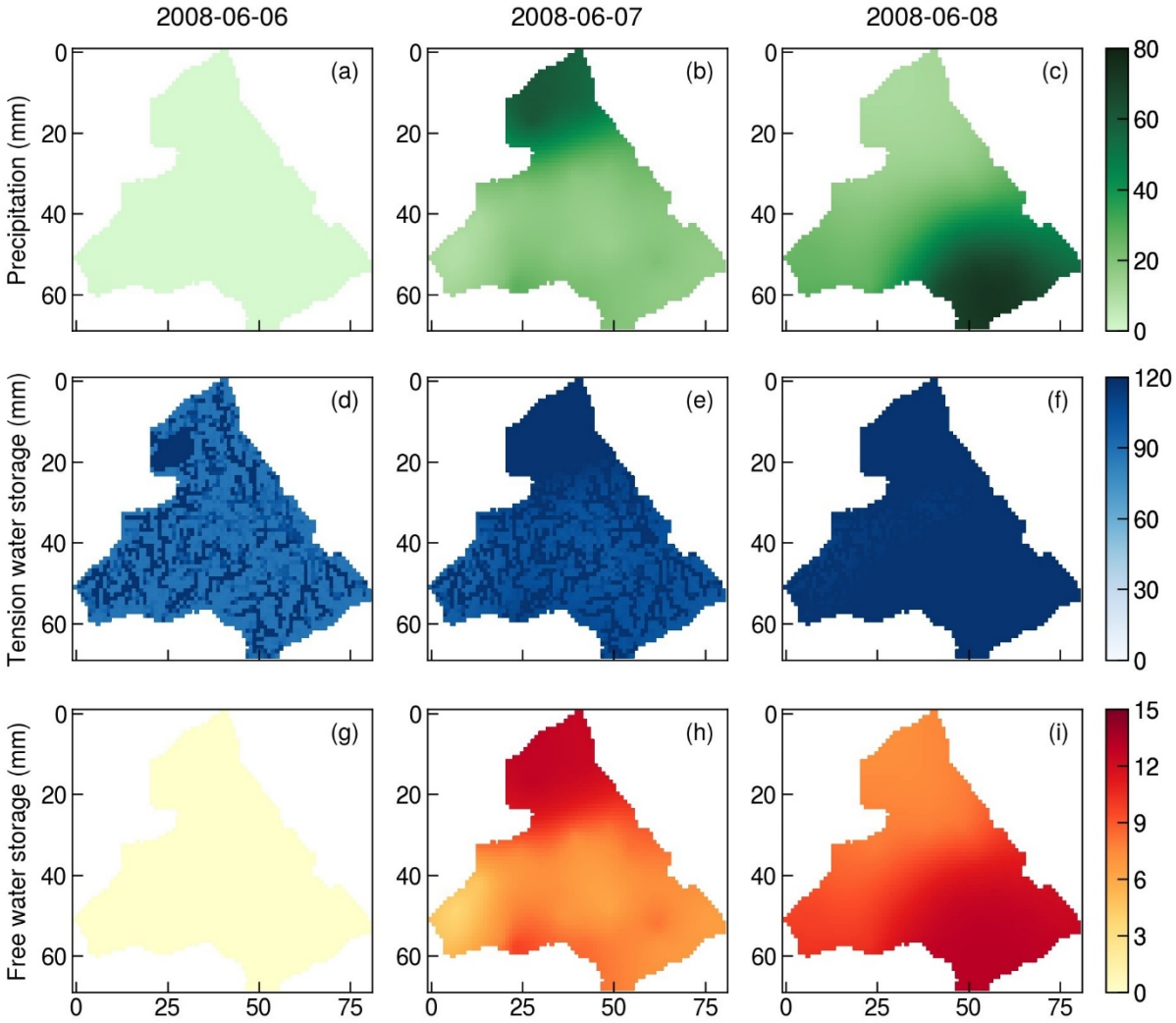

Figure 10. The spatial distribution of precipitation for three days in 2008 (a-c), along with the spatial distribution of tension (d-f) and free water storage (g-i) simulated by TDD-XAJ model for the three days."

11. Line 591-595: In the final paragraph of the conclusion, the authors summarize the limitations of this study. The manuscript encompasses extensive research efforts. I understand that the journey from proposing a model to its refinement and maturity is a lengthy process, and this manuscript has done an excellent job methodologically, providing a solid foundation for future application and research. I recommend relocating this paragraph to the discussion part, where the potential application scenarios and future research directions of the model can be further explored.

Thanks for your encouragement. As suggested, we will add a section in Result and Discussion part of the revised manuscript, which is shown below:

"4.5 Limitations and further research

The main limitation of the TDD-XAJ model is that it addresses only the numerical errors on the time scale from the ODE's numerical solution, while neglecting errors arising from the spatial discretization of the PDE via the FVM method. Future research should consider using methods like manufactured solutions

(Bisht and Riley, 2019) as an alternative for evaluating numerical errors arising from both spatial and temporal discretization when exact solutions are difficult to obtain. Additionally, exploring more advanced spatial discretization techniques—such as second-order FVM or discontinuous Galerkin method (Shaw et al., 2021)—and more sophisticated temporal integration methods could help control numerical errors more effectively.

In terms of computational efficiency, although we make extensive use of the NumPy library—which is generally faster than native Python code— we acknowledge that NumPy may still be slower in certain operations (e.g., element-wise calculations) compared to compiled languages. This is a well-known limitation within the Python community, and solutions like Just-In-Time (JIT) compilation have been proposed (Lam et al., 2015), which convert frequently executed script code into machine code with further automatic optimizations. Although this manuscript primarily focuses on presenting the theoretical aspects of the TDD-XAJ model, we plan to optimize the code—potentially including parallelization—in future work.

It is essential to validate the model with more real-world watershed data and evaluate its uncertainty, particularly for watersheds with varying scales, diverse underlying physical conditions, and hydrological data at different temporal resolutions. The differential-form mathematical equations established for the TDD-XAJ model provide a solid foundation for future research, including combining deep learning for better model parameterization and process understanding (Höge et al., 2022; Li et al., 2024).”

References mentioned in the response

Arcement, G. J. and Schneider, V. R.: Guide for selecting manning's roughness coefficients for natural channels and flood plains, 2339, https://doi.org/10.3133/wsp2339, 1989.

Bisht, G. and Riley, W. J.: Development and verification of a numerical library for solving global terrestrial multiphysics problems, J. Adv. Model. Earth Syst., 11, 1516-1542, https://doi.org/10.1029/2018MS001560, 2019.

Beven, K. J., Kirkby, M. J., Freer, J. E., and Lamb, R.: A history of TOPMODEL, Hydrol. Earth Syst. Sci., 25, 527-549, https://doi.org/10.5194/hess-25-527-2021, 2021.

Chen, J., Chen, J., Liao, A., Cao, X., Chen, L., Chen, X., He, C., Han, G., Peng, S., Lu, M., Zhang, W., Tong, X., and Mills, J.: Global land cover mapping at 30m resolution: A POK-based operational approach, ISPRS-J. Photogramm. Remote Sens., 103, 7-27, https://doi.org/10.1016/j.isprsjprs.2014.09.002, 2015.

Chen, L., Deng, J., Yang, W., and Chen, H.: Hydrological modelling of large-scale karst-dominated basin using a grid-based distributed karst hydrological model, J. Hydrol., 628, 130459, https://doi.org/10.1016/j.jhydrol.2023.130459, 2024.

FAO and IIASA: Harmonized world soil database (version 2.0) [dataset], https://www.fao.org/soils-portal/data-hub/soil-maps-and-databases/harmonized-world-soil-database-v20/en/, 2023.

Fang, Y. H., Zhang, X., Corbari, C., Mancini, M., Niu, G. Y., and Zeng, W.: Improving the Xin'anjiang hydrological model based on mass–energy balance, Hydrol. Earth Syst. Sci., 21, 3359-3375, https://doi.org/10.5194/hess-21-3359-2017, 2017.

Höge, M., Scheidegger, A., Baity-Jesi, M., Albert, C., and Fenicia, F.: Improving hydrologic models for predictions and process understanding using neural odes, Hydrol. Earth Syst. Sci., 26, 5085-5102, https://doi.org/10.5194/hess-26-5085-2022, 2022.

Lam, S. K., Pitrou, A., and Seibert, S.: Numba: a llvm-based python jit compiler, in: Proceedings of the Second Workshop on the LLVM Compiler Infrastructure in HPC, Austin, Texas, 7, https://doi.org/10.1145/2833157.2833162, 2015.

Li, B., Sun, T., Tian, F., Tudaji, M., Qin, L., and Ni, G.: Hybrid hydrological modeling for large alpine basins: a semi-distributed approach, Hydrol. Earth Syst. Sci., 28, 4521-4538, https://doi.org/10.5194/hess-28-4521-2024, 2024.

Liu, J., Chen, X., Zhang, J., and Flury, M.: Coupling the Xinanjiang model to a kinematic flow model based on digital drainage networks for flood forecasting, Hydrol. Process., 23, 1337-1348, https://doi.org/10.1002/hyp.7255, 2009.

Maidment, D. R., Olivera, F., Calver, A., Eatherall, A., and Fraczek, W.: Unit hydrograph derived from a spatially distributed velocity field, Hydrol. Process., 10, 831-844, https://doi.org/10.1002/(SICI)1099-1085(199606)10:6<831::AID-HYP374>3.0.CO;2-N, 1996.

Miao, Q., Yang, D., Yang, H., and Li, Z.: Establishing a rainfall threshold for flash flood warnings in China's mountainous areas based on a distributed hydrological model, J. Hydrol., 541, 371-386, https://doi.org/10.1016/j.jhydrol.2016.04.054, 2016.

Ouyang, W., Ye, L., Chai, Y., Ma, H., Chu, J., Peng, Y., and Zhang, C.: A differentiable, physics-based hydrological model and its evaluation for data-limited basins, J. Hydrol., 649, 132471, https://doi.org/j.jhydrol.2024.132471, 2025.

Perrini, P., Cea, L., Chiaravalloti, F., Gabriele, S., Manfreda, S., Fiorentino, M., Gioia, A., and Iacobellis, V.: A runoff-on-grid approach to embed hydrological processes in shallow water models, Water Resour. Res., 60, e2023WR036421, https://doi.org/10.1029/2023WR036421, 2024.

Seibert, J., Bergström, S., and Sveriges, L.: A retrospective on hydrological catchment modelling based on half a century with the HBV model, Hydrol. Earth Syst. Sci., 26, 1371-1388, https://doi.org/10.5194/hess-26-1371-2022, 2022.

Shaw, J., Kesserwani, G., Neal, J., Bates, P., and Sharifian, M. K.: LISFLOOD-FP 8.0: the new discontinuous Galerkin shallow-water solver for multi-core CPUs and GPUs, Geosci. Model Dev., 14, 3577-3602, https://doi.org/10.5194/gmd-14-3577-2021, 2021.

Shi, G., Sun, W., Shangguan, W., Wei, Z., Yuan, H., Li, L., Sun, X., Zhang, Y., Liang, H., Li, D., Huang, F., Li, Q., and Dai, Y.: A China dataset of soil properties for land surface modelling (version 2, CSDLv2), Earth Syst. Sci. Data, 17, 517-543, https://doi.org/10.5194/essd-17-517-2025, 2025.

Su, B., Kazama, S., Lu, M., and Sawamoto, M.: Development of a distributed hydrological model and its application to soil erosion simulation in a forested catchment during storm period, Hydrol. Process., 17, 2811-2823, https://doi.org/10.1002/hyp.1435, 2003.

Tong, B.: Fine-scale rainfall-runoff processes simulation using grid Xinanjiang (grid-XAJ) model, Hohai University, Nanjing, Jiangsu, 2022.

Yao, C., Li, Z., Yu, Z., and Zhang, K.: A priori parameter estimates for a distributed, grid-based Xinanjiang model using geographically based information, J. Hydrol., 468-469, 47-62, https://doi.org/10.1016/j.jhydrol.2012.08.025, 2012.

Zhao, J., Duan, Y., Hu, Y., Li, B., and Liang, Z.: The numerical error of the Xinanjiang model, J. Hydrol., 619, 129324, https://doi.org/10.1016/j.jhydrol.2023.129324, 2023.

Zhao, R.: The Xinanjiang model applied in China, J. Hydrol., 135, 371-381, https://doi.org/10.1016/0022-1694(92)90096-E, 1992.